IOP Conf. Series: Materials Science and Engineering **418** (2018) 012113 doi:10.1088/1757-899X/418/1/012113

Considering fluctuations of material properties, stainless steel 1.4301, on manufacturability of kitchen sinks

D Harsch[1*], P Fischer[1], B Berisha[2], J Heingärtner[2], Y Renkci[3] and P Hora[1]

[1] ETH Zürich, Institute of Virtual Manufacturing, Tannenstr. 3, 8092 Zürich, Switzerland
[2] inspire AG - ivp, Technoparkstrasse 1, 8005 Zürich, Switzerland
[3] Franke Technology and Trademark Ltd., Hergiswil, Switzerland

E-mail: harsch@ivp.mavt.ethz.ch

Abstract. In production of deep drawn sheet metal parts, it is often challenging to achieve a robust process. Especially in the production of kitchen sinks made out of stainless steel, the fluctuation of the process and material properties often lead to robustness problems. Therefore, numerical simulations are used to detect critical regions. To keep a constant product quality, process control is realised based on metamodels, which are computed by means of a series of finite element simulations. In order to enhance the forecast capability of the simulation model and to increase the reliability of quality features, the yield curve, the yield locus and the forming limit curve (FLC) of different suppliers are measured with tensile, bulge and Nakazima experiments. Because of the large deformation capability of stainless steels, large drawing depths can be achieved. However, the classic Nakazima geometries are not distributed homogenously in the forming limit diagram (FLD). To overcome this shortcoming, a shape optimization of the Nakazima specimen has been performed. Furthermore the influence of alloying elements on the hardening behaviour and on the FLC are analysed. In addition, the measured FLC-T (temperature dependent FLC) conducted with heated Nakazima tests is compared with the computed FLC-T with the modified maximum force criterion (MMFC).

1. Introduction

The kitchen sinks produced by Franke are made out of austenitic stainless steels (1.4301). The material is supplied by three different material suppliers (A, B, C). In this paper, the material behaviour of one batch of material of each company is characterized and compared with each other [1]. Because of the strain-induced martensite the hardening behaviour is strongly temperature dependent. Furthermore the alloying elements influence the martensite formation rate and therefore also the hardening behaviour. In order to characterize the hardening, the Hänsel model is computed based on thermal tensile experiments [2], [3].

In deep drawing simulations, the forming limit curve (FLC) is used as a failure criterion. In order to verify the influence of higher tool temperatures on the FLC, Nakazima tests are conducted with heated tools. The resulting FLC-T (temperature dependent FLC [3]) is then compared with the computed FLC-T using the modified maximum force criterion (MMFC) [4], [5].

During serial production the increasing tool temperature affects the lubrication and therefore also the friction conditions. These effects can be measured with strip drawing tests at various temperature, velocity and pressure levels. The fitted friction model is then used in simulation. The effects of

increasing temperature during serial production or changing material stacks affect the production and thus the product quality. In order to keep a constant part quality, variant simulations are computed. The influences of the material, the temperature and the friction on the quality features are then condensed in metamodels, which form a basis for a subsequent process control [6], [7].

2. Hardening behaviour

The hardening behaviour of stainless steel is strongly temperature dependent because of the temperature dependent martensite formation rate. The strain-induced martensite is very typical for metastable austenitic CrNi materials during cold forming at temperatures below 80°C. By conducting material experiments at different temperature levels, the martensite volume and the hardening behaviour can be measured. Then, the parameters of the Hänsel model are fitted with the measured tensile experiments in rolling direction at 0, 10, 20, 40, 60 and 80°C and a strain rate of 0.002 s^{-1} [2].

The base function of the Hänsel model (see Equation (2)) is fitted with the Hockett-Sherby (HS) equation at the reference temperature of 80°C. At this temperature, the material stays austenitic and no martensite is formed during deformation. The influence of the temperature on the austenitic flow curve is taken into account with a linear function (see Equation (3)). The actual martensite volume is calculated by the integration of the martensite formation rate over the strain path [2]. The contribution of martensite volume fraction to the flow stress is taken into account by a linear relation given by a parameter Δk_f in Equation (1).

$$\sigma(\varphi, T, V_M) = \sigma_{HS}(\varphi) \cdot f(T) + \Delta k_f^{\gamma \to \alpha'} \cdot V_M \quad (1)$$

$$\sigma_{HS}(\varphi) = B_{HS} - (B_{HS} - A_{HS}) \cdot e^{-m \cdot \varphi^n} \quad (2)$$

$$f(T) = [1 - K \cdot (T - T_{ref})];\ T_{ref} = 80°C \quad (3)$$

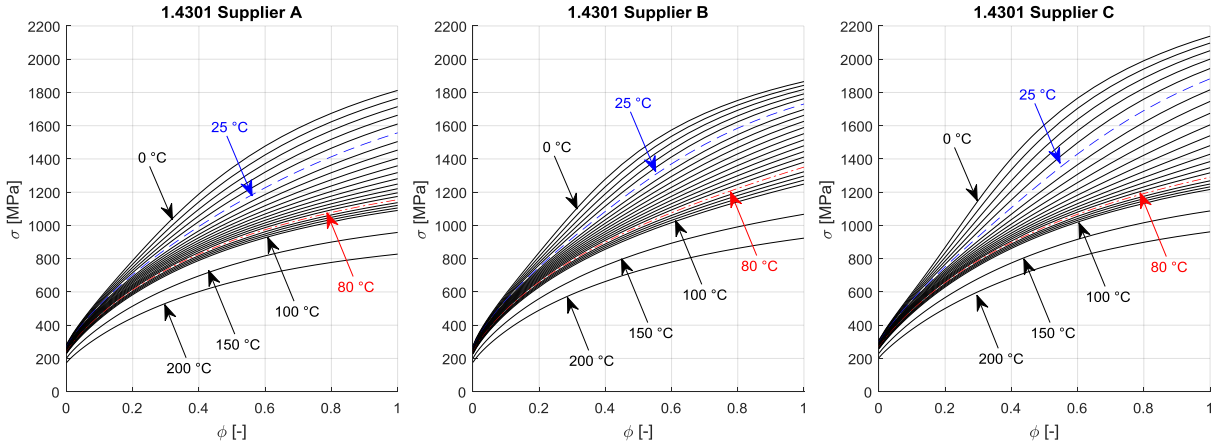

Figure 1. Isothermal hardening curves (Hänsel model) for 1.4301 of A, B and C.

Table 1. Parameters of the Hänsel model.

	B_{HS}	A_{HS}	m	n	K	$\Delta k_f^{\gamma \to \alpha'}$
A	1318 MPa	239.9 MPa	1.80	0.90	0.002288	459.0 MPa
B	1444 MPa	240.0 MPa	1.70	0.86	0.001977	441.3 MPa
C	1485 MPa	268.2 MPa	1.70	0.92	0.002037	402.2 MPa

The data of the bulge experiment cannot be used for a better extrapolation behaviour of the base model [8], because it is not conducted at 80°C, thus martensite is generated during room temperature bulge testing [1]. The martensite content is measured during the tensile experiments. Because the permeability of the martensite differs under load (Villari effect), the measured martensite content does

not correspond to the real martensite volume. By conducting tensile experiments with cyclic releases to zero stress at different temperatures and strain values, the Villari effect can be modelled with the approximation function of Krauer [3].

The possibilities in AutoForm are limited to implement thermal material behaviour, especially parameters of the Hänsel model. Therefore isothermal hardening curves are used in a look-up table in AutoForm, as they are shown in Figure 1 [1]. The major disadvantage of this method is the information about the actual martensite volume integrated over the strain and temperature path gets lost. In AutoForm parameters of the Hänsel model cannot be modified, because they are hard-coded. Thus the evaluated martensite volume is only a post variable and does not affect the hardening behaviour of the material.

2.1. Influence of alloying elements on hardening behaviour

The properties of stainless steel are affected by different alloying elements, heat treatment and impurities. According to the standard, austenitic stainless steel 1.4301 consists of chromium between 17 – 19.5%, nickel between 8 – 10.5%, manganese less than 2.0% and additional alloying elements. Nickel is added to promote an austenitic microstructure and increases ductility, toughness (ability to absorb energy) and to reduce the corrosion rate. Furthermore it is also used to form the intermetallic compounds, which increase strength [9]. The production of nickel is highly resource-intensive, consequently the amount is reduced to a minimum. Manganese is acting as an austenite stabiliser at low temperatures. It is used as an austenite former and can also replace some of the nickel. Conversely, molybdenum slightly increases mechanical strength and promotes the formation of secondary phases [9]. Of each material supplier, two batches of different melts are used to compare the chemical composition and the resulting material properties (see **Table 2** and **Table 3**). All values are measured by the material supplier themselves according to the standard DIN EN ISO 6892-1.

Table 2. Amount of alloying elements of different material suppliers of 1.4301.

[%]	Batch	C	Mn	Si	P	S	Cr	Ni	Mo	N
A	A1	0.037	1.22	0.330	0.030	0.001	18.02	9.03	0.280	0.026
	A2	0.040	1.26	0.320	0.030	0.001	18.11	8.53	0.180	0.053
B	B1	0.040	1.21	0.58	0.032	0.001	18.40	8.00	-	0.053
	B2	0.034	1.27	0.50	0.033	0.001	18.10	8.10	-	0.041
C	C1	0.050	1.02	0.397	0.029	0.004	18.11	8.05	-	0.044
	C2	0.060	1.03	0.423	0.032	0.004	18.04	8.04	-	0.030

Table 3. Material characteristics of the different batches (1.4301).

	Batch	$\sigma_{0.2}$ [MPa]	σ_{TS} [MPa]	A_{80} [%]
A	A1	230	614	63.0
	A2	269	615	60.0
B	B1	272	637	60.6
	B2	285	642	62
C	C1	270	666	53.0
	C2	287	647	55.2

The influence of the alloying elements on the corresponding material specifications are depicted in Figure 2 as pairs of values. Nickel reduces the yield stress and along with manganese it also decreases the tensile strength. Whereas manganese increases ductility and thus elongation at break A_{80}. The material from supplier C contains the minimum amount of nickel and less manganese, thus austenite is less stabilised and more martensite is formed during deformation. This leads to a reduced ductility.

At 80°C no martensite is formed, hence the yield curves of the three materials are purely austenitic (Figure 3 left, from the Hänsel model). The material from A clearly shows a smaller hardening compared to the two other suppliers, probably caused by different heat treatment. The hardening curve of A at 50°C corresponds to the ones of C and B at 80°C. The same effect can be observed between A at 30°C and C at 50°C. The main reason for this is the significantly lower martensite formation during deformation, which is depicted in Figure 3 as martensite volume integrated over the strain at constant temperatures. Hence, the stabilising effect of martensite is decreased for A.

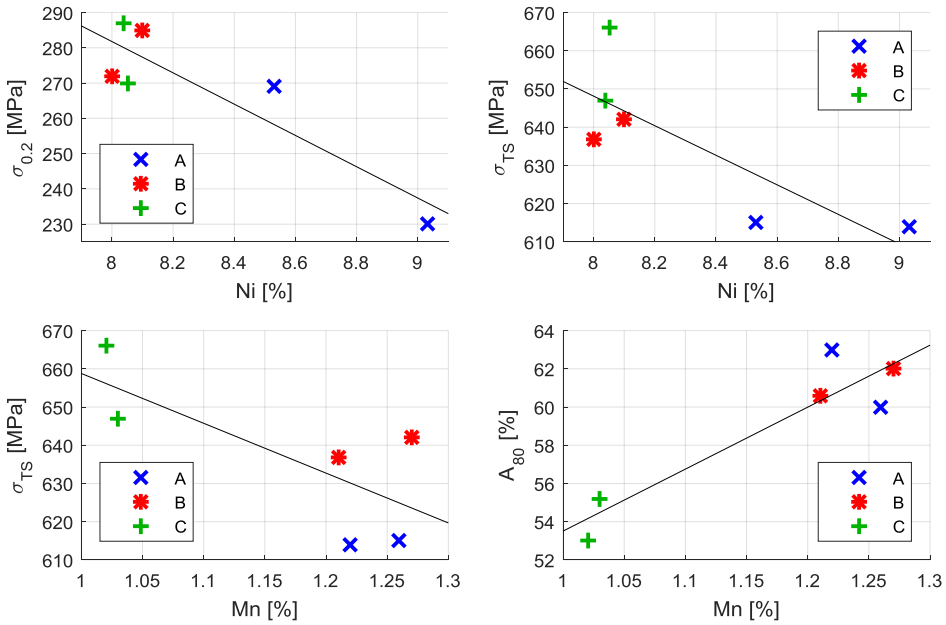

Figure 2. Dependency of material properties of alloying elements.

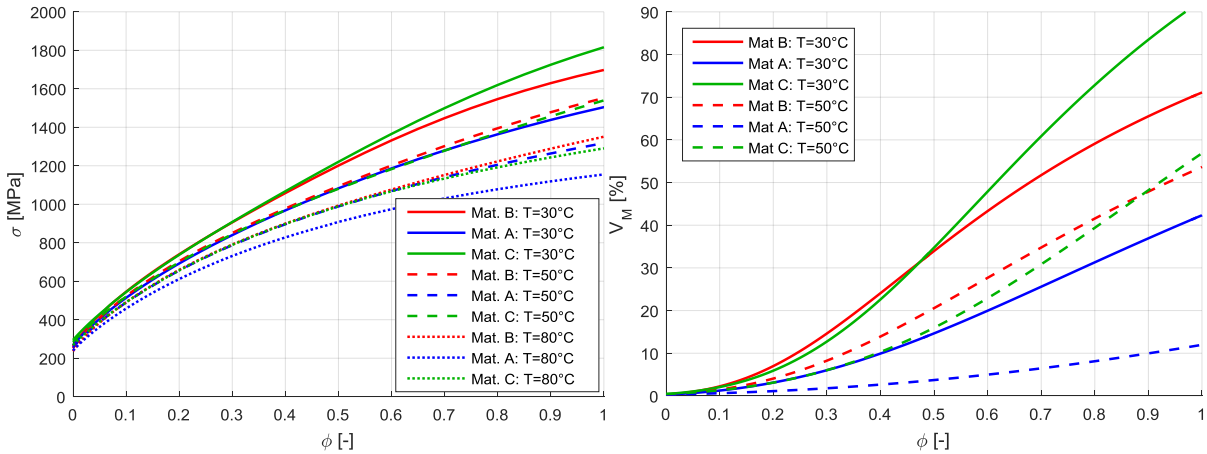

Figure 3. Hardening curves and predicted martensite volume for isothermal deformation (Hänsel model).

The shown martensite volumes are significantly higher than other values in the literature [2], [3]. The measurement system Fischerscope, which is calibrated with ferrite calibration samples, measures an equivalent amount of ferrite. Because of the difference in permeability between martensite and ferrite, the measured values have to be adjusted by a factor of 1.7 to get the correct amount of martensite [10]. Probably in [2] and [3] this effect might not be taken into account. Other deviations can result from the material supplier, the material batch and the temperature increase due to higher strain rate.

During kitchen sink production, the tool temperatures can easily increase up to 50°C, which can actually lead to an error-prone production due to the material behaviour (of course also because of changing friction conditions). Especially when changing the batch of material or worse the material supplier, the process needs to be adjusted in order to obtain the same part quality.

3. Yield locus

To obtain the yield locus, tensile experiments in 0°, 45° and 90° to rolling direction were conducted at room temperature. In each direction the r-values and yield stress are measured. Furthermore bulge tests are used to capture the biaxial stress state, which is evaluated at 4% of logarithmic strain in order to reduce the uncertainties at the beginning of the bulge test [8]. The biaxial values at 4% equivalent strain are then converted to equivalent strains of 0% plastic deformation based on the uniaxial values at 4% and the rule of three. For larger strains the temperature increase in the bulge test strongly differs from the tensile experiment, which leads to different martensite contents and thus to a non-proportional evolution of the uniaxial to the biaxial stress. In order to make a comparison at higher strains, both specimen should contain the same amount of martensite at the identical equivalent strain. The M-value of the yield locus is assumed to be 8 because of the face-centered cubic crystal structure, which leads to better results compared to 6 [3]. The biaxial anisotropy is evaluated in the biaxial Nakazima experiment (B200) and bulge test, which is practically 1. In comparison to the stack compression test, Nakazima and bulge test always lead to a biaxial anisotropy of close to 1 because of the strain constraints. The measured and assumed values are shown in Table 4, which are used to calculate the BBC yield locus [11].

Table 4. Measured values for yield loci at room temperature.

	r_0	r_{45}	r_{90}	r_b	σ_0	σ_{45}	σ_{90}	σ_b	M
A	0.773	1.180	0.876	1	269.9	253.5	258.6	271.5	8
B	0.754	1.261	0.852	1	263.8	249.3	251.1	246.6	8
C	0.861	1.333	0.807	1	297.6	279.2	282.4	296.3	8

4. Forming limit curve

4.1. Measuring FLC with Nakazima tests

The FLCs for the materials A and C in Figure 4 are measured with the standardised Nakazima experiments and evaluated with the strain-rate dependent method [11], whereby the supposed uniaxial experiment B20 has been removed, because in Nakazima test the boundary condition differs from the tensile experiment. This leads to significantly different necking behaviour [4]. The Nakazima samples B50, B80, B90, B100 and B120 are nearly on one line with an angle of 45°. This corresponds to the Hill localised instability theory [13].

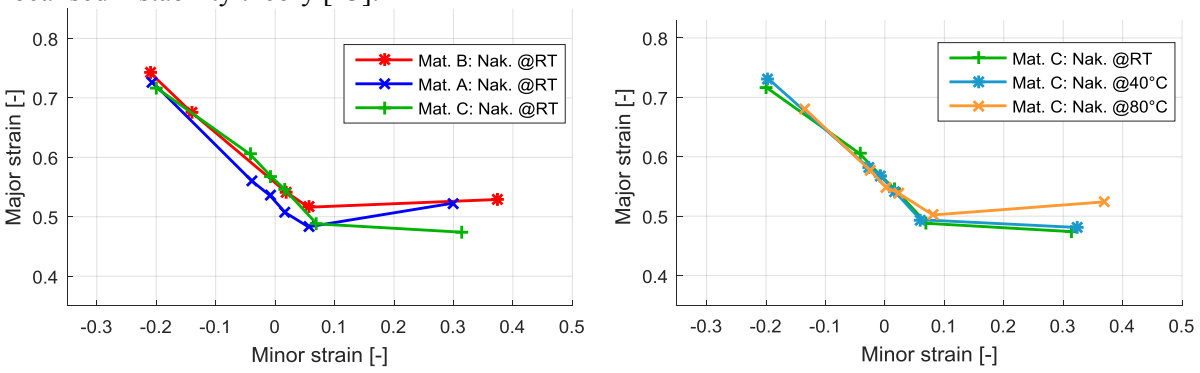

Figure 4. Measured FLCs with Nakazima tests (left: all materials at room temperature, right: FLC-T).

For the material C the FLC-T is measured at room temperature, 40°C and 80°C to analyse the effect of higher temperature on the failure criterion. During serial production the tool temperature is increasing. Hence, Nakazima tests are conducted with heated tools without pre-heating of the sample (lies at least 30 seconds on binder). Between plane strain and uniaxial tensile test the FLCs are nearly identical. Thus, in this region the FLC seems not to be affected by increasing tool temperatures. On the contrary, localisation occurs later for higher tool temperatures (80°C) for biaxial stress, similar to material A, which forms less martensite. One possible explanation for this effect is that ductility is reduced when large amounts of martensite are formed. By taking triaxiality into account, martensite formation is beneficial in a biaxial stress state [14]. This leads to lower localisation strains for biaxial stress state at lower temperature. Contrarily the decreasing mean flow stress at elevated temperature increases the elongation at fracture [15], [16].

The Nakazima experiments for B have been reduced to the specimens B50, B100, B120 and B200 because of the linear behaviour between plane strain and uniaxial stress state. In order to verify the straight line between B50 and B120, a novel geometry has been optimised to reach a point between B50 and B80 based on the approach of [17] in AutoForm Sigma and tested. The geometry and the strain path of the experiment are depicted in Figure 5. Furthermore the reproducibility of the experimental results, especially of the localisation on top, is improved compared to the other Nakazima samples. The resulting point (mean value of 3 samples) in the FLD confirms the linear behaviour for negative minor strains (see Figure 4). The experiments have been conducted with very small and sharp drawbeads. This leads to a smaller biaxial pre-stretching compared to the Nakazima experiments conducted with standard drawbeads.

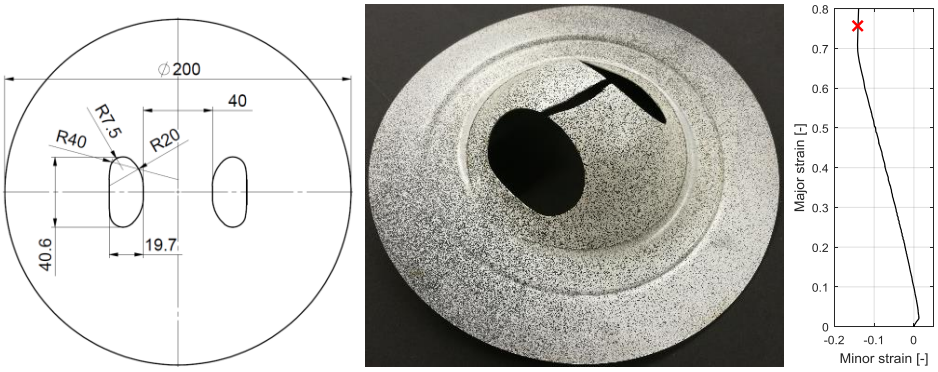

Figure 5. Nakazima experiment with modified sample geometry.

The Nakazima experiment B200 at room temperature (without pre-heating the tools) of material C is measured with an infrared camera during deformation. The temperature increases from 25°C up to 45°C. For 12 stages distributed over the testing time, temperature and strain values are measured on top of the sample. The points are plotted in Figure 6. Based on these values, the martensite volume is integrated over the strain and increasing temperature. The resulting martensite content is very similar to the isothermal martensite formation at 25°C during the first 35 seconds of the experiment. With increasing temperature, less martensite is formed, thus the deviation to the isothermal martensite (blue line) increases. The last point of the integrated martensite volume from the Hänsel model (red line) is then compared with the measured martensite after the experiment (red asterisk). The calculated martensite fraction shows a very good accordance to the measurement. Therefore the model of martensite formation rate in the Hänsel model has a sufficient accuracy, whereby additional strain paths (e.g. B50 and B120) should be analysed using the same method.

The higher temperature on the outer surface of the specimen, which can be seen in Figure 6 left after 35 seconds as a green ring, is caused by the plastic work. Compared to the centre of the specimen, the contact with the punch is missing. Thus, heat transfer is limited and the temperature increases where the tool contact is missing. At the end of the experiment, the strain rate increases significantly. Thereby the

generated heat due to deformation increases the temperature of the specimen because of the limited heat dissipation.

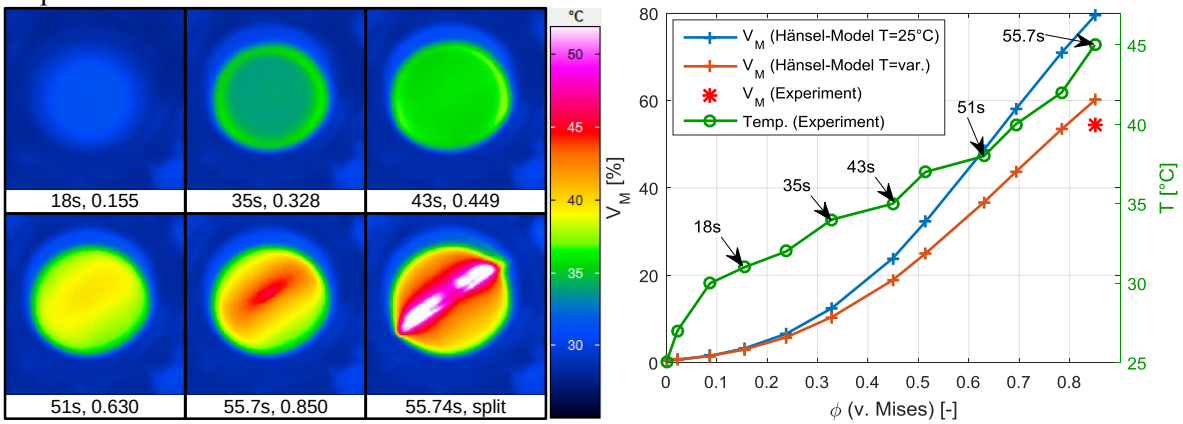

Figure 6. Nakazima experiment B200: Temperature increase and martensite integration.

During the Nakazima test, the temperature increases (see Figure 6), which influences the martensite formation rate. During the first part of the experiment, martensite is formed. Due to the plastic work the temperature increases and less martensite is formed towards the end of the experiment compared to a constant temperature. This leads to a hardened material with martensite but with less formability compared to pure austenitic material. Thus, the material breaks at lower strains. This effect is only observed in biaxial direction. One reason is the significantly higher equivalent strain in the biaxial direction compared to all other Nakazima samples.

4.2. Evaluation with MMFC

The modified maximum force criterion is evaluated based on the isothermal flow curves of the Hänsel model at 30°C and the yield loci at room temperature, whereby the adapted yield loci are all fitted with the BBC model. For high M-values the MMFC method runs into numerical instabilities, if the yield locus does not exhibit a sufficient curvature in plane strain direction. Therefore a substitute M_{crack} value of 2 is used instead. All computed FLCs with MMFC contain a biaxial pre-strain of 5%, because of the biaxial pre-strain in the experiments through the imprint of the drawbead when closing the die with the binder and because of the initial deformation at the beginning of drawing through the punch in the centre of the specimen.

The MMFC evaluated for material A (Figure 7 left) at 30°C leads to acceptable results for a quick estimation of the FLC. Contrarily the MMFC method used on material C at 30°C is much higher. Also the evaluation at higher temperatures predicts a wrong behaviour. Possible reasons for this effect are mentioned in section 4.1 regarding martensite formation, but also the use of a different yield locus exponent M_{crack} does affect the results.

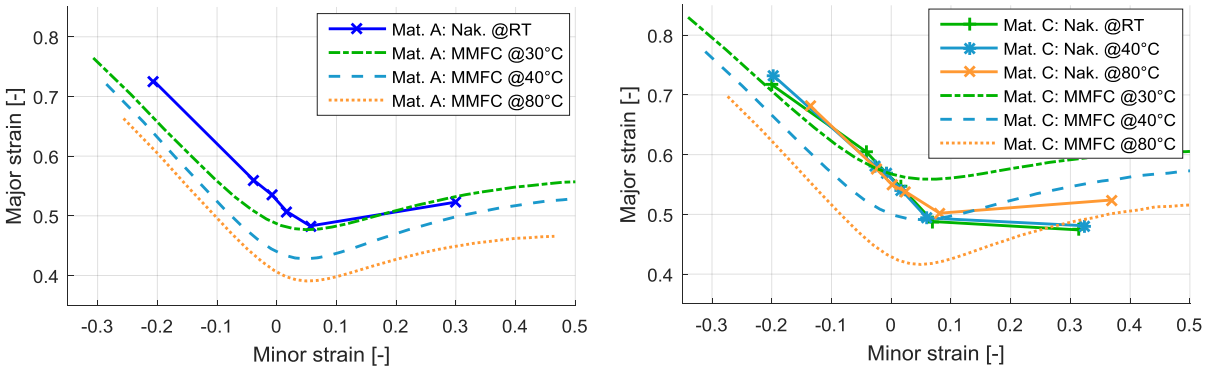

Figure 7. Evaluation of MMFC compared to Nakazima experiments (left: A, right: C).

5. Friction Model

In order to measure the temperature, velocity and pressure dependency, strip drawing tests are conducted [3]. The commonly used friction models from AutoForm and Grüebler are then fitted with the experimental data [1], [11], [18]. The effect of friction models on the simulation result is compared with the standard Coulomb friction model. For the purpose of comparable results, following procedure is carried out (see [1]):

1. Digitise representative part from serial production (e.g. with GOM ATOS [1])
2. Use all known properties of production in simulation
3. Calibrate draw-in in simulation with digitised part (minimisation of draw-in difference) by means of a correction factor (for each friction model)
4. Validate the simulated material thickness with the digitised material thickness from step 1 (for each friction model)

The calibration of the friction model is performed to compensate the software specific contact formulation. The Coulomb friction coefficients in e.g. LS-Dyna are much smaller compared to AutoForm to obtain the same simulation results. Furthermore all other effects, which are not taken into account, such as the unknown tool stiffness, are also partially compensated through the calibration. Figure 8 depicts on the left the thickness distribution of the digitised part, which was measured with the GOM ATOS system. On the right side the result variable thickness of the calibrated AutoForm simulation with a Coulomb friction coefficient of 0.07 is shown.

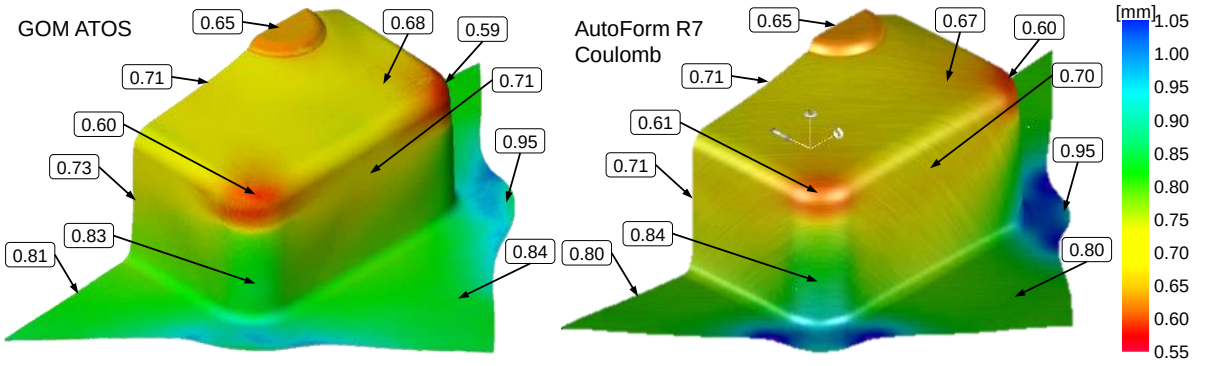

Figure 8. Thickness distribution of digitised part (left) and AutoForm simulation (right)

The difference of the thickness distribution between the simulations with different friction models is very small (less than 0.01 mm) and are not generating any advantage compared to the calibrated Coulomb friction model. The AutoForm model only takes the pressure and velocity dependency into account. The reference velocity in the friction model by AutoForm is based on the smallest, measured velocity of 20 mm/s as recommended by [3]. Smaller velocities do not influence the friction. Thus, friction in simulations with velocities below 20 mm/s (which is very typical for kitchen sink production with a ram velocity between 10 – 30 mm/s) is only pressure dependent. Therefore the friction model in AutoForm is not generating any benefit. The friction model by [18] only takes influences from changes in temperature and velocity into account. The corresponding simulation result only shows minor differences in regions with large deformations, where temperature increases due to higher deformation energy. Overall, for simulation of kitchen sinks with ram velocities below 30 mm/s a standard Coulomb friction model is sufficient. It is more important to calibrate the friction coefficient by means of aligning the draw-in from simulation with the measured draw-in of a part from production.

6. Conclusion and Outlook

The amount of alloying elements in stainless steels (1.4301) varies considerably between the different suppliers. This leads to significantly disparate material behaviour, especially in strain-induced martensite formation. Higher amounts of nickel and manganese increase the stabilisation of austenite,

thus less martensite is formed and the ductility is increased. A higher ductility does not automatically lead to an increased robustness of the kitchen sink production, because the drawing process is stabilised through the local formation of martensite.

The FLC computed with the MMFC provides a good approximation at room temperature for materials with low martensite formation. For materials with higher martensite formation the deformation energy leads to a temperature increase, and consequently to a reduced martensite content compared to the isothermal flow curve. Consequently the standard MMFC method predicts larger deformation to failure. This effect could be taken into account by considering an adiabatic temperature increase in the MMFC method [3].

Acknowledgment
The authors are very grateful to the CTI (The Swiss Innovation Promotion Agency) for the financial support of this work within the project 17366.1 PFIW-IW. Also thanks to Franke Group for providing the material. The project partner AutoForm Engineering GmbH and GOM International AG are also gratefully acknowledged for their contribution on the project results. Additionally Prof. Dr. Ton van den Boogaard is thankfully acknowledged for the fruitful discussions.

References

[1] D. Harsch, J. Heingärtner, Y. Renkci, P. Hora. Influence of scattering material properties on the robustness of deep drawing processes, FTF 2017.
[2] A. Hänsel. Nichtisothermes Werkstoffmodell für die FE-Simulation von Blechumformprozessen mit metastabilen austenitischen CrNi-Stählen. Diss. ETH Nr. 12672, 1998.
[3] J. Krauer. Erweiterte Werkstoffmodelle zur Beschreibung des thermischen Umformverhaltens metastabiler Stähle. Diss. ETH Nr. 19070, ISBN 978-3-18-367602-6, 2010.
[4] P. Hora, B. Berisha, M. Gorji, H. Hippke. Modelling of Instability and Fracture Effects in Sheet Metal Forming Based on Extended X-FLC Concept. Trans. Tech. Publ. Switzerland, 2016.
[5] P. Hora, L. Tong, N. Manopulo. Theoretical prediction of FLC based on curvature and strain rate dependent MMFC criterions. IDDRG, Proceedings, 2016.
[6] P. Fischer, D. Harsch, J. Heingärtner, Y. Renkci, P. Hora. Inline feedback control for deep drawing applications. The International Deep Drawing Research Group, Proceedings, 2016
[7] P. Fischer , D. Harsch, J. Heingärtner, Y. Renkci, P. Hora. A knowledge-based control system for the robust manufacturing of deep drawn parts. Int. Conf. of Tech. of Plasticity, ICTP 2017.
[8] P. Peters. Yield functions taking into account anisotropic hardening effects for an improved virtual representation of deep drawing processes. Diss. ETH Nr. 22707, 2015.
[9] Outokumpu, Website: http://www.outokumpu.com/en/products-properties, February 2018.
[10] G. Heinemann. Virtuelle Bestimmung des Verfestigungsverhaltens durch verformungsinduzierte Martensitbildung. Diss. ETH Nr. 15846, 2004.
[11] AutoForm R7.0.2 Software Manual. AutoForm Engineering GmbH, February 28, 2017.
[12] W. Volk, P. Hora. New algorithm for a robust user-independent evaluation of beginning instability for the experimental FLC determination. Int. Journal of Material Forming, 2011
[13] R.M. Wagoner, K.S. Chan, S.P. Keeler. FLD – Concepts, Methods, Applications, TMS, 1989.
[14] A.H. van den Boogaard. Including triaxiality in the Hänsel model for martensite evolution. ETH Zürich, Technical Report, 2008.
[15] S.M. Hussani, S.K. Singh, A.K. Gupta. Experimental and numerical investigation of formability for austenitic stainless steel 316. Journal of Material Research Technology, 2014.
[16] H. Takuda, K. Mori, et. al. Finite element analysis of the formability of an austenitic stainless steel sheet in warm deep drawing. Journal of Materials and Processing Tech., 2003.
[17] D. Banabic, L. Lazarescu, D.S. Comsa. An Innovative Procedure for the Experimental Determination of the Forming Limit Curves. Book: 60 Excellent Inventions in Metal Forming, Pages 11-16, 2015.
[18] R. Grüebler. Simulation des umformtechnischen Tribosystems. Diss. ETH Nr. 14883, 2002.